2012 2nd International Conference on Power and Energy Systems (ICPES 2012)
IPCSIT vol. 56 (2012) © (2012) IACSIT Press, Singapore
DOI: 10.7763/IPCSIT.2012.V56.12

Synthesis of ZnO Hollow Nanospheres and Their Electrochemical Reactivity for Lithium-ion Batteries

Sasidharan Manickam [1+], Nanda Gunawardhana [2] and Masaki Yoshio [3]

[1] SRM Research Institute, SRM University, Kattankulathur, Chennai 603203, India.
[2] International Research Center, Senate Building, University of Peradeniya, Peradeniya, 20400, Sri Lanka
[3] Advanced Research Center, Saga University, 1341 Yoga–machi, Saga 840–0047, Japan

Abstract. ZnO hollow nanosphere of size about 32 ± 2 nm is reported using polymeric micelle with *core-shell-corona* structure as a soft-template. Poly(styrene–*b*–acrylic acid–*b*–ethylene oxide) micelles (PS–PAA–PEO) with anionic *shell* block facilitates the formation of hollow nanospheres through electrostatic interaction of Zn^{2+} with $–COO^–$ ions followed by precipitation/deposition reaction under mild alkaline conditions. X-ray diffraction (XRD) analysis confirmed the formation of pure ZnO phase (Zincite-type) with hexagonal lattice-structure (P_{63mc}). Transmission electron microscope (TEM) confirmed the existence of hollow spherical structure with average diameter of 32 ± 2 nm. The hollow particles were also thoroughly characterized by SEM, EDX, FTIR, nitrogen adsorption, and thermal analyses by TG/DTA. The electrochemical characteristics of ZnO hollow nanospheres as anode materials for lithium ion battery are investigated and the obtained results are also compared with dense granular powders. The hollow nanosphere based electrode delivers high initial discharge capacity of 1304 $mAh.g^{-1}$ at a charge/discharge rate of 0.25 C. More importantly, the nanoconstructed electrodes maintain the structural integrity even after subjecting to high current density.

Keywords: ZnO hollow nanospheres, Micelles, Anode materials, Good cycling performance

1. Introduction

Metal oxides are potential alternatives to graphite as anode materials of lithium ion batteries as they can deliver much higher reversible capacities even at high current densities. Among the different metal oxides, ZnO has some advantages, for example, low cost, easy preparation and scalability, and high chemical stability. As an anode material of lithium ion batteries, ZnO has a theoretical capacity of 978 $mAh.g^{-1}$ [1]; however, it is rarely investigated in the lithium-ion battery field since it suffered from poor electrochemical kinetics and severe capacity fading upon cycling and huge volume change [2-5]. The important reason is that ZnO is a material with low conductivity, and the electrode made from ZnO often suffers the loss of electrical contact arising from the large volume change during the repeated discharge-charge processes. In order to circumvent these obstacles, the electrochemical properties of ZnO was improved by coating with Ni, C, Mg, or NiO-C layers [6,7] and preparing ordered nanostructured materials [2,8,9].

Generally, it is believed that when material sizes are reduced down to nanometer scale, usually exhibit significantly enhanced functionalities in their properties. For instance, hollow nanoparticles with spherical morphology are unique candidates with high mechanical strength, surface permeability, and high surface area. Hollow nanospheres with thin shell domain not only enhance the fast lithium insertion/deinsertion kinetics but also the hollow void could serve as an effective buffering medium [10]. Recently, we have reported the fabrication TiO_2, La_2O_3 and V_2O_5 hollow nanospheres using anionic polymeric micelles with *core-shell-corona* architecture [11-13]. Herein, we report the fabrication of ZnO hollow nanospheres using

+ Corresponding author. +91-44-2741-7912; fax: +91-44-2745-6702.
E-mail address: sasidharan.m@res.srmuniv.ac.in

anionic micelles through electrostatic interaction of Zn^{2+} ions with anionic micelles followed by precipitation under mild alkaline conditions. ABC triblock copolymer poly(styrene–*b*–acrylic acid–*b*–ethylene oxide)

(PS-PAA-PEO) with anionic COO^- was used as a template and $Zn(OAc)_2$ was used as metal source. The hollow nanospheres were characterized by TEM, XRD, FTTR, SEM/EDX, thermal analysis with TG/DTA and nitrogen sorption analyses. The electrochemical characteristics of ZnO hollow nanospheres were further investigated as anode materials for rechargeable lithium-ion batteries.

2. Experimental

The fabrication of hollow zinc oxide nanospheres with micelles of poly(styrene-*b*-acrylic acid-*b*-ethylene oxide (PS–*b*–PAA–*b*–PEO) using zinc accetate as metal precursor was carried out as follows. Polymeric micelles solution was prepared by dissolving the required amount of the above polymer in distilled water and then transferred to a volumetric flask to obtain a stock solution with a concentration of 0.5 gL^{-1}. The micelle solution was adjusted to pH 9 by using dilute NaOH solution. On addition of zinc salt solution, the clear micelle solution slowly turns to turbid due to formation of $Zn(OH)_2$ in *shell* domain of micelles and the contents were gently stirred for overnight at room temperature using a magnetic stirrer. The synthesis protocol was tuned by changing the ratio of Zn^{2+}/PAA between 5 and 10 to obtain monodispersed hollow nanospheres. The composite particles were repeatedly washed with distilled water and ethanol and dried at 60 ℃ to remove moisture. In order to remove the polymeric template as well as to crystallize the ZnO hollow particles, the composite particles were calcined at 500 ℃ for 4 h in a muffle furnace under air.

Hydrodynamic diameter (D_h) of the template micelles of PS–PAA–PEO was measured with an Otsuka ELS–800 instrument. Wide-angle X-ray diffraction (WXRD) patterns were recorded using CuK_α radiation with a Shimadzu XRD-7000 diffractometer. The textural properties such as BET surface area and mesopore–size distribution were obtained using nitrogen adsorption/desorption isotherms with a BELSORB instrument. The morphology of the samples was observed from JEOL TEM–1210 (acceleration voltage: 80 KV) and JEOL TEM–2100 electron microscopes (acceleration voltage: 200 KV). FTIR spectra were recorded on a Jasco FTIR-7300 spectrometer. TG and DTA analyses were carried out using MAC Science TG–DTA 2100. Energy dispersed X-ray analysis was carried out with Hitachi S-3000N.

For lithium insertion studies, the zinc oxide hollow nanosphere (5 mg) was mixed mechanically with teflonized acetylene black (TAB–2, 3 mg) and then the mixture was pressed on a stainless steel mesh as the current collector under a pressure of 500 kg/cm^2 and dried at 160 ℃ for 4 hours under vacuum. The electrochemical characterizations were carried out using CR–2032 coin type cells with lithium as an anode. The electrolyte used was 1M $LiPF_6$–EC: DMC (1:2 volume ratios, Ube Chemicals Co. Ltd.). The coin cell assembling was performed in a glove box filled with argon (dew point, lower than −80 ℃). The galvanostatic charge–discharge tests of the coin cell were performed at the constant current density of 0.5 $mAcm^{-2}$. The cyclic voltammograms (CV) were recorded with a Hokuto Denko HSV–100 in a beaker type cell containing zinc oxide hollow nanospheres as working electrode and a lithium foil as a counter and reference electrodes. The charge–discharge performance was carried out in the voltage range of 3.0–0.05 V.

3. Results and Discussion

The hydrodynamic diameter D_h (67 nm) and the ζ–potential (–56 mV) of the micelles (pH 9) were obtained from dynamic light scattering (DLS) and electrophoretic light scattering (ELS) experiments, respectively. Nearly monodispersed spherical micelles with average diameter *ca*. 46 ± 1 nm estimated from TEM image (not shown) were used as template for fabrication hollow nanospheres. The difference in the micelle particle's size between DLS and TEM is due to the fact that the latter accounts for only the *core-shell* part and excludes *corona* part of the micelle [11-13]. The TG/DTA analyses of ZnO/polymer composite particles revealed that all the organic contents were decomposed between 200 and 420 ℃ (not shown) and the total organic content was found to be 16.2 %. Thus the calcination step is essential to create a hollow void space by removing the core-domain of polymeric micelles. The absence of C–H, –C=C–, and –COOH bond stretching vibrations of phenyl groups of polymer backbone in the FTIR spectrum of the calcined sample (not shown) is also consistent with the thermal analyses [14]. The phase purity and crystallinity of zinc oxide hollow nanospheres was investigated by powder X-ray diffraction (XRD). Comparison of wide-

angle X-ray diffraction (WXRD) patterns of zinc oxide nanospheres (after calcination) and composite particles (before calcination) (Figure 1) suggested highly pure zincite crystalline phase. All diffraction peaks can be indexed as the hexagonal phase of ZnO with the lattice constants a = 0.325 nm and c = 0.521 nm, which is in good agreement with the JCPDS data, No. 36-1451.

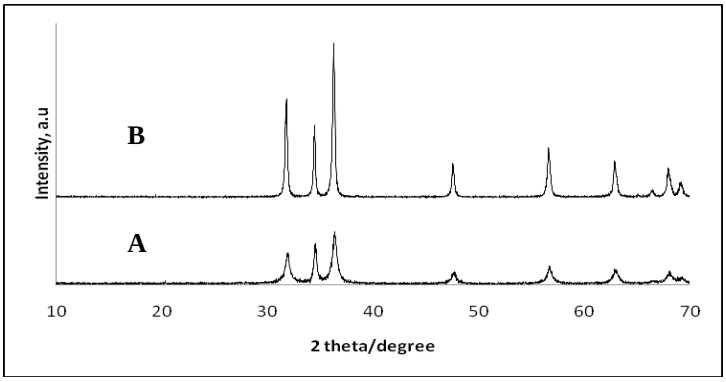

Fig. 1: Powder X-ray diffraction patterns of: (A) ZnO-composites and (B) ZnO hollow nanospheres.

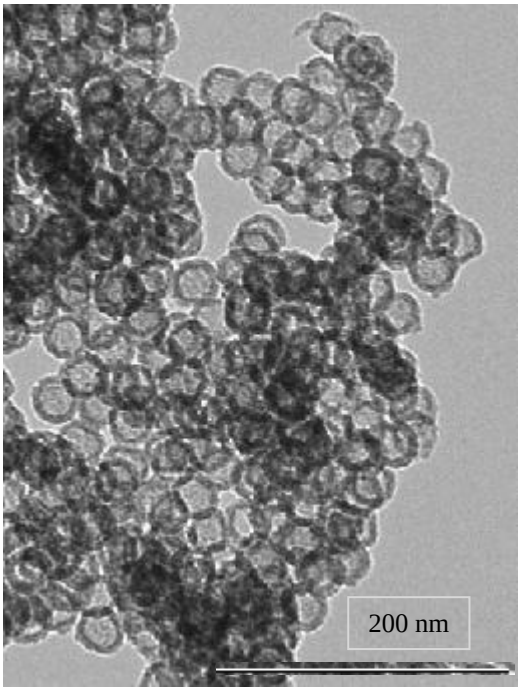

Fig. 2: TEM image of ZnO hollow nanospheres (Zn^{2+}/PAA = 8)

Figures 2 exhibits TEM image of material with Zn^{2+}/PAA mole ratio of 8. The average particle size and void space diameter were found to be 32 ± 2 and 18 ± 1 nm, respectively. The wall thickness estimated by TEM (Figure 2) was approximately 7 ± 1 nm. However, at lower Zn^{2+}/PAA ratios (Zn^{2+}/PAA = 3 and 5), the degree of aggregation of nanospheres is relatively low compared to Zn^{2+}/PAA 10, due to deposition of zinc precursor species outside micelle domain. Furthermore, the PS block core size estimated from the TEM observation was found to be 23 ± 1 nm; however, after calcinations the void space diameter was approximately 18 ± 1 nm due to shrinkage. In addition, for hollow particles with high precursor concentration (Zn^{2+}/PAA = 10), the shell thickness increased marginally to 8 ± 1 nm. In addition, the pore size distribution curves based on BJH model showed disordered mesopores. The total pore volume and BET surface area were found to be 0.59 cm^3g^{-1} and 119 m^2g^{-1}, respectively. The high-resolution transmission electron microscope (HRTEM, not shown) allows the resolution of lattice fringes of the crystals to be correlated to the (110) planes of the zincite lattice structure. Furthermore, energy-dispersive X-ray

spectroscopy spectrum (EDX, not shown) shows strong peaks for zinc and oxygen suggestive of the pure zinc oxide phase confirming the highly pure zinc oxide hollow nanospheres.

Figure 3A exhibits the cyclic voltammograms (CV) of ZnO hollow nanospheres measured between 0 and 3 V at a scan rate of 3 mV/min. In the first cathodic scan, there is a major strong peak at 0.23 V and a minor peak at 0.57 V, which are related to the electrochemical process of the ZnO material. This process contains the reduction of ZnO into Zn, the formation of Li-Zn alloy, and the growth of the gel-like solid electrolyte interphase (SEI) layer. The potentials of these reactions are very close, so it shows one major broad peak and a minor shoulder. In the first anodic scan, the four peaks located at 0.38 (broad), 0.51, 0.68, and 1.37 V are attributed to the multi-step dealloying process of Li-Zn alloy [2, 15]. The second cathodic sweep differs from the first one; the major peak at 0.23 V is vanished and new peaks at 0.4 and 0.72 V (broad) were appeared for the second cycles. The anodic peaks of the second cycle, however, are more similar to that of first cycle according to literature [16].

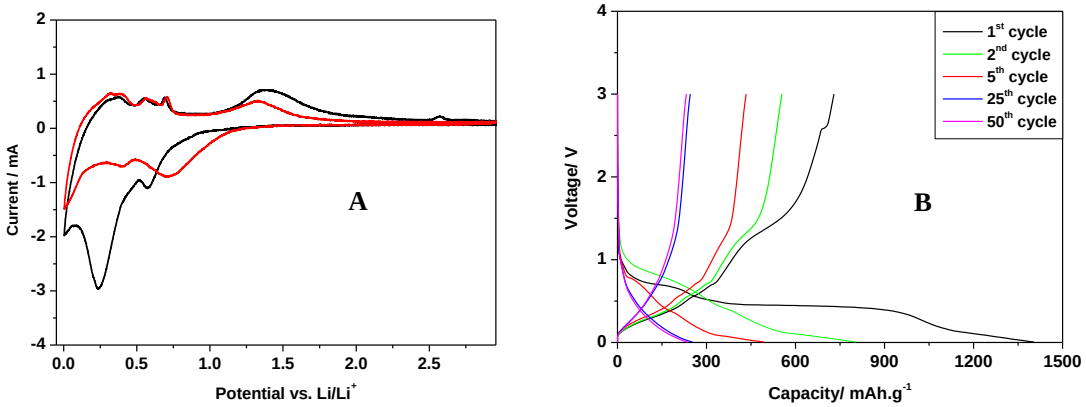

Fig. 3: (A) CV curves of ZnO hollow nanospheres in 1.0 m $LiPF_6$ (EC/DMC = 1/2 (v/v)) at a 3 mV/min sweep rate and (B) The Charge/discharge profiles ZnO hollow nanospheres at 0.25 C rate in the voltage region of 0.005-3.0 V.

Figure 3B shows discharge-charge curves in the voltage window of 0.005–3.0 V (vs. Li) at a rate of 0.25 C up to 50 cycles and for clarity, only selected cycles are shown in the voltage versus capacity profiles. It is worth to note that the plateaus on the voltage profiles coincide with the cathodic and anodic peaks in the CV curves (Fig.3A). A very obvious long plateau located at about 0.5 V appears in the first discharge curve. However, in the first charge curve, the plateaus are not so obvious. It can be seen four slopes, which are located at 0.28, 0.45, 1.33, and 2.5 V, respectively. After the first cycle, the slopes in discharge curves are around 0.8 and 0.4 V, and the curves are similar in shape, indicating that the reactions become more reversible. The ZnO hollow nanospheres deliver a first discharge capacity of 1304 $mAh.g^{-1}$, and a first charge capacity of 730 $mAh.g^{-1}$. It is important to mention that the very high discharge-capacity observed in the first cycle must originate from electrolyte decomposition in the low-potential region and subsequent formation of solid electrolyte interphase (SEI) on the hollow nanospheres [17]. The discharge capacities of the ZnO hollow particles based electrode (Fig.4) in the 1^{st}, 2^{nd}, 5^{th}, 25^{th}, and 50^{th} cycles are 1304, 804, 494, 252 and 249 mAh g^{-1}, respectively. The corresponding charge capacity values are 730, 554, 434, 251, and 248, mAh g^{-1} for the 1^{st}, 2^{nd}, 5^{th}, 25^{th}, and 50^{th} cycles, respectively. The coulombic efficiency of first cycle was found to be 62.5 %. However, the dense ZnO powder exhibited significantly lower charge-discharge capacities (not shown) compared to ZnO hollow nanospheres under similar experimental conditions. For instance, the discharge capacities of ZnO dense particles are 471, 352, 214, 151, and 144 $mAh.g^{-1}$ for 1^{st}, 2^{nd}, 5^{th}, 25^{th}, and 50^{th} cycles; whereas the corresponding charge capacities were found to be 275, 210, 162, 141, 139 $mAh.g^{-1}$ for 1^{st}, 2^{nd}, 5^{th}, 25^{th}, and 50^{th} cycles, respectively.

Fig.4A shows the capacity versus cycle number plot for ZnO hollow nanospheres. As can be seen, both discharge and charge capacities decrease up to 10 cycles and thereafter the capacity stabilizes. After 100 cycles with 100 % depth of discharging and charging at a rate of 0.1 C, the electrode capacity decreased to 246 mAh g^{-1}. After about 10 cycles, the columbic efficiency, the ratio of discharge/charge capacity is nearly

100 %. However, cycle performance of dense ZnO particles was poor as the discharge capacities reduced from 1090 to 118 mAh.g^{-1} within a few cycles of repeated charge/discharges (not shown). Fig. 4B shows the rate performance of ZnO hollow nanospheres. At a low rate of 0.1 C, hollow particles show a discharge capacity of about 1414 mAh g^{-1}. However, the discharge capacities gradually decrease to 306, 195, and 116 mA g^{-1} at 1C, 5C and 10C, respectively. However, the ZnO hollow particle based electrodes almost regains their original high-capacities when the rate was again lowered to 0.1 C after being exposed to high current loads (10 C), which indicates the high stability of hollow nanospheres based electrodes. The improved electrochemical performance is attributed to the unique hollow spherical morphology. More importantly, the void space not only effectively buffers against charge storage and local volume change but also provides better electrical contact and shorter diffusion path length providing better rate capability.

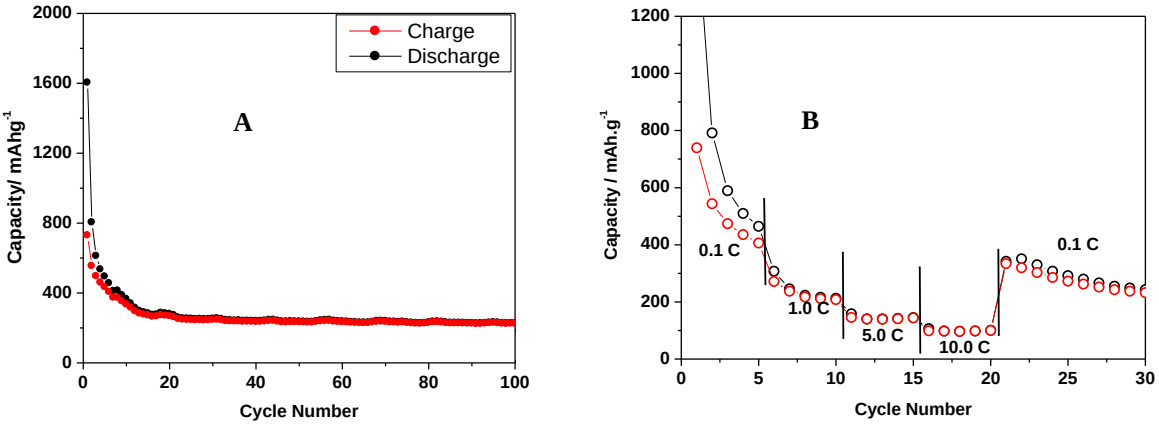

Fig. 4: (A) Charge-discharge cycling performance ZnO hollow nanospheres at 0.1 C rate in the voltage region of 0.005-3.0 V vs. Li/Li$^+$ and (B) Rate performance in the voltage region of 0.005-3.0 V.

4. Conclusions

Core-shell-corona micelle obtained from poly(styrene-*b*-acrylic acid-*b*-ethylene oxide) successfully produce ZnO hollow nanosphere of size about 32 ± 2 nm. TEM, SEM/EDX, and XRD analyses confirmed the formation of hollow nanospheres and purity or crystallinity of ZnO nanoparticles. ZnO hollow nanospheres exhibited good cycling performance even after 100 cycles of repeated charge/discharges and the discharge capacity at 100th cycle was found to be 246 mAh g^{-1}. The ZnO hollow nanospheres based electrode exhibited high rate capability and cycling performance than the dense ZnO particles. The void space not only act as buffer medium against charge storage and local volume change but also provides better electrical contact and shorter diffusion path length and therefore provide better rate capability.

5. Acknowledgment

Dr. M. Sasidharan thanks JSPS for Research Grant to carry out the research.

6. References

[1] C.Q. Zhang, J.P. Tu, Y.F. Yuan, X.H. Huang, X.T. Chen, F. Mao, *J. Electrochem. Soc*. 2007, **154:** A65.

[2] J.P. Liu, Y.Y. Li, X.T. Huang, G.Y. Li, Z.K, Li, *Adv. Funct. Mater*. 2008, **18**, 1448.

[3] Z.W. Fu, F. Huang, Y. Zhang, Y. Chu, Q.Z. Qin, *J. Electrochem. Soc*. 2003, **150,** A714.

[4] F. Belliard, P.A. Connor, J.T.S. Irvine, *Ionics* 1999, **5**, 450.

[5] J.P. Liu, Y.Y. Li, R.M. Ding, J. Jiang, Y.Y. Hu, X.X. Ji, Q. B, Chi, Z.H. Zhu, X.T. Huang, *J. Phys. Chem. C* 2009, **113,** 5336.

[6] G.F. Yan, H.S. Fang, G.S. Li, L.P. Li, H.J. Zhao, Y. Yang, Chin. *J. Struct. Chem*. 2009, **28,** 409.

[7] X. Tang, Q. Pan, J. Liu, *J. Electrochem. Soc*. 2010, **157,** A55.

[8] P. Poizot, S. Laruelle, S. Grugeon, L. Dupont, J.M. Tarascon, *Nature* 2000, **407,** 496.

[9] M.N. Obrovac, R.A. Dunlap, R.J. Sanderson, J.R. Dahn, *J. Electrochem. Soc*. 2001, **148,** A576.

[10] M. Sasidharan, K. Nakashima, N. Gunawardhana, T. Yokoi, M. Inoue, S. Yusa, M. Yoshio, T. Tatsumi, *Chem. Commun*.**,** 2011, **47**, 6921.

[11] M. Sasidharan, N. Gunawardhana, M. Inoue, S. Yusa, M. Yoshio, K. Nakashima, *Chem. Commun*. 2011, **48**, 3200.

[12] M. Sasidharan, N. Gunawardhana, H. N. Luitel, T. Yokoi, M. Inoue, S. Yusa, T. Watari, M. Yoshio, T. Tatsumi, K. Nakashima, *J. Colloid and Interface Science*, 2011, **370**, 51.

[13] M. Sasidharan, N. Gunawardhana, M. Yoshio, K. Nakashima, *J Electrochemical Soc.* 2012, **159**, A618.

[14] M. Sasidharan, K. Nakashima, N. Gunawardhana, T. Yokoi, M. Ito, M. Inoue, S. Yusa, M. Yoshio, T. Tatsumi, *NanoScale*, 2011, **3**, 4768.

[15] F. Belliard, J.T.S. Irvine, *J. Power Sources*, 2001, **97-98**, 219**.**

[16] X.Z. Huang, X.H. Xia, Y.F. Yuan, F. Zhou, *Electrochimica Acta*, 2011, **56**, 4960.

[17] W. B. Xing, J. R. Dahn, *J. Electrochem. Soc*. 1997, **144,** 1195.